






Combining physics-informed neural networks with the freezing mechanism for general Hamiltonian learning

Leonardo K. Castelano ^{1,*} Iann Cunha ¹ Fabricio S. Luiz ^{2,3} Reginaldo de Jesus Napolitano,⁴
Marcelo V. de Souza Prado ⁵ and Felipe F. Fanchini ^{5,6}

¹*Departamento de Física, Universidade Federal de São Carlos (UFSCar), São Carlos 13565-905, São Paulo, Brazil*

²*Federal Institute of São Paulo, Itapetininga 18202-000, São Paulo, Brazil*

³*Instituto de Física Gleb Wataghin, Universidade Estadual de Campinas, Campinas 13083-859, São Paulo, Brazil*

⁴*São Carlos Institute of Physics, University of São Paulo, P.O. Box 369, São Carlos 13560-970, São Paulo, Brazil*

⁵*Faculty of Sciences, UNESP - São Paulo State University, Bauru 17033-360, São Paulo, Brazil*

⁶*QuaTI - Quantum Technology & Information, São Carlos 13560-161, São Paulo, Brazil*



(Received 1 November 2023; accepted 22 August 2024; published 6 September 2024)

The precision required to characterize a Hamiltonian is central to developing advantageous quantum computers, providing powerful advances in quantum sensing and crosstalk mitigation. Traditional methods to determine a Hamiltonian are difficult due to the intricacies of quantum systems, involving numbers of equations and parameters that grow exponentially with the number of qubits. To mitigate these shortcomings, in this paper, we introduce an innovative and effective procedure integrating a physics-informed neural network (PINN) with a freezing mechanism to learn the Hamiltonian parameters efficiently. Although PINN and experimental data alone would become impractical as N increases, the mechanism we introduce freezes the interactions of most of the qubits, leaving just a qubit subsystem to be analyzed by the PINN method. Determination of all physical parameters is accomplished by analyzing the system by parts until completion. We validated the efficacy of our method using simulation data obtained from the IBM quantum computer to obtain the training data and we found that a PINN can learn the two-qubit parameters with high accuracy, achieving a median error of less than 0.1% for systems of up to four qubits. We have successfully combined the PINN analysis of two qubits with the freezing mechanism in the case of a four-qubit system.

DOI: [10.1103/PhysRevA.110.032607](https://doi.org/10.1103/PhysRevA.110.032607)

I. INTRODUCTION

The promise of a revolution in computational capabilities impels an ever-growing investment in the development of quantum computers. Precise characterization of the Hamiltonian describing such a machine is a prerequisite to the promised quantum advantage. Obtaining the Hamiltonian parameters from experimental data is the main challenge due to the intrinsic high dimensions and complexity of interconnected quantum systems. Several methods to allow Hamiltonian learning have been proposed [1–10]. A recent approach involves learning Hamiltonians through derivative estimation [11]. While this method represents substantial progress, it is limited to sparsely interacting Hamiltonians.

In Sec. II, we describe the methodology, focusing on the integration of physics-informed neural networks (PINNs) with the freezing mechanism. Section III provides analytical solutions for the freezing mechanism. In Sec. IV, we discuss the practical implementation of general Hamiltonian learning. In Sect. V, we present numerical results and error analysis, demonstrating the accuracy of our method. In Sec. VI, we apply our approach to data obtained from the IBM quantum

computer. Finally, Sec. VII concludes the paper; we summarize our findings and discuss potential future applications.

II. METHODOLOGY: COMBINING PINNS WITH THE FREEZING MECHANISM

In this work, we introduce the concept of the freezing mechanism (FM), a technique that allows isolating qubits within a quantum system. We demonstrate that the FM combined with PINNs offers a powerful approach for Hamiltonian learning. The PINN concept has been leveraged so that differential equations describing the physics of the problem are integrated into the training of the neural network [12–14]. This approach offers the advantage of reducing the amount of training data required, as the neural network is constrained to satisfy the differential equations that adhere to physical laws [12–14]. Furthermore, the idea of learning and extracting information from a collection of data can also be implemented through the inverse-PINN method [12–14]. In this case, data are provided along with the equations and physical parameters can be extracted from the model.

In principle, however, while we could apply the inverse-PINN method to determine all the parameters of an N -qubit Hamiltonian, the number of differential equations grows exponentially with N . Due to the limitations of current computational power to solve the N -qubit Hamiltonian directly

*Contact author: lkcastelano@df.ufscar.br

by the PINN method, we provide a practical solution that relies on a piecewise analysis of the whole system. Thus, the Hamiltonian of a subsystem can be learned and this procedure can be repeated until all parameters are obtained. The success of our approach comes from a technique, based on the continuous dynamical decoupling [15–19], which is used to isolate a particular subset of q qubits from N qubits, as we explain in the following.

In this paper, we combine the FM with the inverse-PINN method to achieve comprehensive learning of general Hamiltonians for N qubits:

$$H_0 = -\frac{1}{2} \sum_{k_1, k_2, \dots, k_N=0}^3 J_{k_1, k_2, \dots, k_N} (\sigma_{k_1}^{(1)} \sigma_{k_2}^{(2)} \dots \sigma_{k_N}^{(N)}). \quad (1)$$

The notation $\sigma_k^{(j)}$ denotes that the Pauli matrix σ_k acts only on the j th qubit and leaves all other qubits intact, for $k = \{0, 1, 2, 3\}$, where σ_0 corresponds to the identity matrix. In principle, we could apply the inverse-PINN method to determine all the coefficients of Eq. (1), but the number of differential equations grows exponentially as 4^N . Due to the lack of the current computational power to solve the N -qubit Hamiltonian directly by the PINN method, we provide a practical solution that relies on a piecewise analysis of the whole system. For example, the Hamiltonian of a subsystem can be learned and this procedure can be repeated until all terms are obtained. Based on continuous dynamical decoupling [15–19], we can isolate a particular set of q qubits from N qubits. The difference from our approach to continuous dynamical decoupling relates to the qubits where external fields are applied. In the continuous dynamical decoupling, external fields act on the qubits of interest at specific time intervals. Here, external fields are applied to qubits in order to disconnect their interactions with the qubits of interest, and the requirement of specific instants of time is no longer necessary.

III. ANALYTICAL SOLUTIONS FOR THE FREEZING MECHANISM

Here, we provide analytical solutions for external fields that, by selectively freezing the dynamics of m ($m < N$) qubits, transform an N -local Hamiltonian as Eq. (1) into a q -local ($q = N - m$) Hamiltonian. First, we rewrite Eq. (1) in such a way that operators related to the m qubits are separated from the rest; thus,

$$H_0 = H_m + H_q, \quad (2)$$

where H_m is the part of the general Hamiltonian that contains all terms incorporating interactions with the m qubits selected to be frozen. The term H_q contains all interactions among the q qubits of interest, excluding those related to the m qubits. The total Hamiltonian includes the freezing Hamiltonian $H_F^m(t)$ and H_0 ; thus,

$$H_{\text{tot}} = H_0 + H_F^m(t), \quad (3)$$

where

$$H_F^m(t) = \sum_{j=1}^m H_s^{(j)}(\omega_j, t). \quad (4)$$

The freezing Hamiltonian for m qubits is the summation over all individual terms, each given by

$$H_s^{(j)}(\omega_j, t) = \left[i \frac{d}{dt} U_s^{(j)}(\omega_j, t) \right] U_s^{(j)\dagger}(\omega_j, t), \quad (5)$$

with

$$U_s^{(j)}(\omega_j, t) = \exp(-i\omega_j t \sigma_3^{(j)}) \exp(-i2\omega_j t \sigma_1^{(j)}). \quad (6)$$

As detailed in Appendix A, this form for the single-qubit evolution operator is chosen to freeze the m selected qubits dynamically. To understand the action of the freezing Hamiltonian [Eq. (5)], we employ the interaction picture. The total Hamiltonian written in this representation is

$$H_I(t) = [U_F^m(t)]^\dagger H_{\text{tot}} U_F^m(t), \quad (7)$$

where the freezing unitary operator $U_F^m(t)$ is the product of the individual evolution operators. Therefore,

$$U_F^m(t) = U_s^{(1)}(\omega_1, t) U_s^{(2)}(\omega_2, t) \dots U_s^{(m)}(\omega_m, t). \quad (8)$$

In the interaction representation, the time-evolution equation becomes

$$i \frac{\partial |\Psi_I(t)\rangle}{\partial t} = [U_F^m(t)]^\dagger H_0 U_F^m(t) |\Psi_I(t)\rangle. \quad (9)$$

It is important to notice that, in the FM, the total interaction-picture Hamiltonian decomposes into

$$[U_F^m(t)]^\dagger H_0 U_F^m(t) = [U_F^m(t)]^\dagger H_m U_F^m(t) + H_q, \quad (10)$$

where terms involving only the q qubits of interest are invariant under the freezing unitary transformation represented in Eq. (8) since they commute with $U_F^m(t)$. We can write a time-evolution operator for $H_I^m(t) = [U_F^m(t)]^\dagger H_m U_F^m(t)$ that satisfies the equation of motion

$$i \frac{\partial U_I^m(t, 0)}{\partial t} = H_I^m(t) U_I^m(t, 0). \quad (11)$$

The Dyson series derived from the above equation is

$$U_I^m(t, 0) = \mathbb{1} - i \int_0^t dt' H_I^m(t') + \frac{(-i)^2}{2} \int_0^t dt' \int_0^{t'} dt'' \mathcal{T}[H_I^m(t'), H_I^m(t'')] + \dots, \quad (12)$$

where \mathcal{T} is the time-ordering operator. By following the result in Appendix A, we have that $U_I^m(t, 0) \approx \mathbb{1}$, for an appropriate choice of the magnitude of the freezing Hamiltonian and the duration of the time evolution. Therefore, we can conclude that $H_I^m(t) \approx 0$ and that Eq. (9) effectively becomes equivalent to

$$i \frac{\partial |\Psi_I(t)\rangle}{\partial t} \approx H_q |\Psi_I(t)\rangle. \quad (13)$$

Because the freezing external fields only act on the m qubits selected, the above equation is equivalent to an equation for isolated $q = N - m$ qubits, whose dynamics are now dictated by a q -local Hamiltonian, H_q . In Fig. 1, we provide a scheme to visualize the FM. In Fig. 1(a), red spheres represent qubits connected to their next neighbors through interactions with similar magnitude. In Fig. 1(b), blue spheres represent the

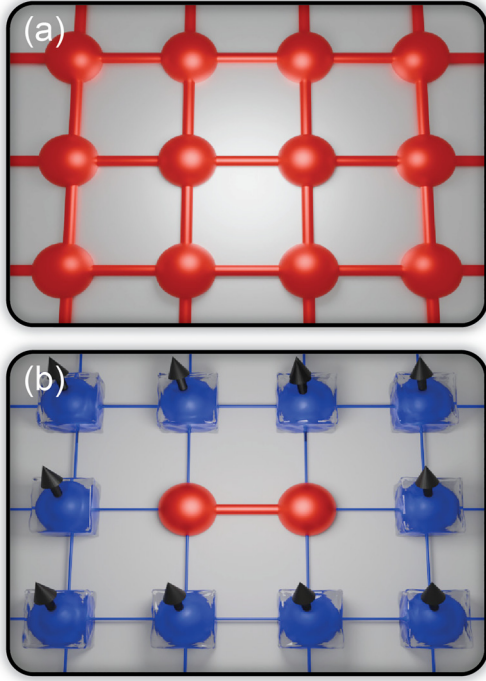


FIG. 1. Schematic picture of the freezing mechanism. We represent qubits by red spheres and their interaction with the connectors. In panel (a), the qubits interact with next neighbors with couplings with the same order of magnitude. In panel (b), we illustrate the FM by blue spheres inside ice cubes. Local external fields, represented by the black arrows, are applied to the chosen qubits; we intend to freeze their interactions with any other qubit. The remaining two red spheres represent the qubits, whose Hamiltonian can be learned by the inverse-PINN method.

frozen qubits, whose interactions with their neighbors are drastically diminished by the local external applied fields. The remaining two red spheres represent a two-qubit system, whose Hamiltonian can be learned using the inverse-PINN method. The coupling interaction between any pair of qubits is likewise obtained by freezing the other interactions.

IV. PRACTICAL IMPLEMENTATION OF GENERAL HAMILTONIAN LEARNING

To understand all the procedures mentioned above, we chose a two-qubit system as the smaller unit for learning all the parameters characterizing a Hamiltonian of N qubits. In general, 16 $J_{k,l}$ terms describe the two-qubit subsystem. The term $J_{0,0}$ only provides a reference for the energy and we set it equal to zero, without loss of generality. The experimental data can be achieved through the expected value for an observable, which is defined as

$$\langle \sigma_{k_1}^{(1)} \sigma_{k_2}^{(2)} \rangle(t) = \text{Tr}[\rho(t) \sigma_{k_1}^{(1)} \sigma_{k_2}^{(2)}], \quad (14)$$

where $k_1, k_2 \in \{0, 3\}$ and $\rho(t)$ is the density matrix for two qubits at time t . The dynamics of the observables is the quantity that is included in the inverse PINN through the

Heisenberg equation

$$\frac{d\langle \hat{O}_m \rangle(t)}{dt} = i\langle [H, \hat{O}_m] \rangle, \quad (15)$$

where H is the Hamiltonian in Eq. (1) for $N = 2$. We adopt the system of units where $\hbar = 1$. The differential equation for $\langle \hat{O}_m \rangle$ is implemented for all 15 physical terms corresponding to $\sigma_{k_1}^{(1)} \sigma_{k_2}^{(2)}$ different from identity. We end up with 15 coupled ordinary differential equations that must be solved for a given initial condition, which we set as $|+\rangle^{(1)} |+\rangle^{(2)}$, with $|+\rangle = (|0\rangle + |1\rangle)/\sqrt{2}$.

The idea behind the inverse-PINN method is to model the solutions of the differential equations by a neural network and to minimize the loss function. Particularly, the loss function can be written as

$$L = L_{\text{model}} + L_{\text{data}}, \quad (16)$$

where

$$L_{\text{model}} = \sum_{m=1}^{15} \sum_{n=1}^{N_c} \left| \left(\frac{d\langle \hat{O}_m \rangle}{dt} - i\langle [H, \hat{O}_m] \rangle \right) \Big|_{t_n} \right|^2. \quad (17)$$

The loss function associated with the model L_{model} finds the values of $\langle \hat{O}_m \rangle$ at N_c collocation points in time; consequently, the solutions of the differential equations are represented by the neural network when L_{model} is zero. Here, collocation points refer to the points in time where the observables are probed. The loss function $L_{\text{data}} = \sum_{m=1}^{15} \sum_{n=1}^{N_c} |\langle \hat{O}_m^{\text{exp}} \rangle(t_n) - \langle \hat{O}_m \rangle(t_n)|^2$ uses data provided by the experiment, denoted by $\langle \hat{O}_m^{\text{exp}} \rangle(t_n)$. This loss function imposes the extra constraint for the solutions of the differential equations to fit the experimental data at the N_c collocation points. In this sense, the inverse-PINN method forces the neural network to simultaneously solve the differential equations and represent the experimental data. To satisfy both requirements, the physical parameters J_{k_1, k_2} must be learned to minimize the total loss function.

V. NUMERICAL RESULTS AND ERROR ANALYSIS

We analyze the number of points of experimental data needed. To perform such a task, we provide data without errors by numerically solving Eq. (15) considering the values of the parameters J_{k_1, k_2} randomly sorted between $[-\omega_0, \omega_0]$, where $\omega_0 = 2\pi/T$ and T is the final time of evolution. The accuracy of our results is measured through the mean absolute percentage error (MAPE), which is defined as follows:

$$\text{MAPE} = \frac{1}{D} \sum_{j=1}^D \frac{|P_j^{\text{exact}} - P_j^{\text{pred}}|}{|P_j^{\text{exact}}|}, \quad (18)$$

where D is the number of physical parameters sampled, and P_j^{exact} (P_j^{pred}) denotes the j th exact (predicted) physical parameter. In Fig. 2(a), we plot the MAPE as a function of the number of collocation points in time for a two-qubit Hamiltonian. We use $D = 750$ samples of random values for the parameters hereafter and the boxplot method to show the spread of the data. In Fig. 2(a), the lowest (highest) marker shows the lowest (highest) data point in the data set excluding any outliers, which are data points that differ significantly

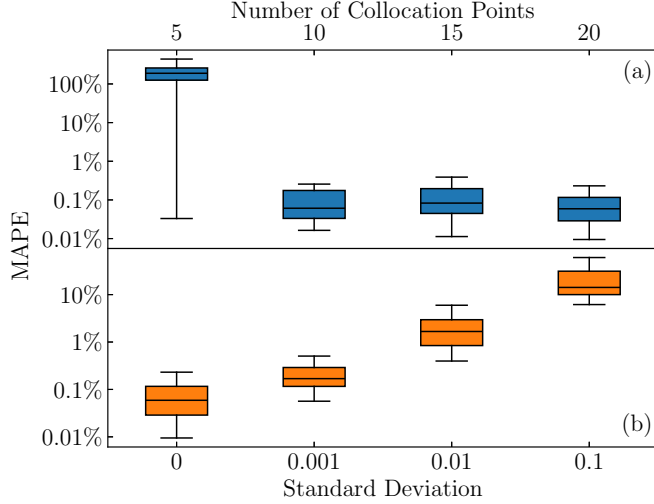


FIG. 2. The MAPE as a function of the number of collocation points (a). The MAPE as a function of the standard deviation for $N = 20$ collocation points (b). Both panels are related to the general two-qubit Hamiltonian and are plotted in logarithmic scale.

from other observations. The lowest (highest) marker in the blue box is related to the lower (higher) quartile and the marker inside the blue box indicates the median. Figure 2(a) demonstrates that the median of the MAPE is lower than 0.1% for $N_c = 20$ collocation points. To further analyze the performance of the Hamiltonian learning, we add a random error drawn from a Gaussian distribution in the observables. In this case, each experimental data for $\langle O_m \rangle(t_n)$ is modified according to $\langle O_m \rangle(t_n) \rightarrow \langle O_m \rangle(t_n) + N(0, \sigma^2)$, where $N(0, \sigma^2)$ is the normal distribution with zero mean and standard deviation σ . In Fig. 2(b), we use $N_c = 20$ collocation points and we include the random Gaussian error in the input data. In this case, we can see that the median of the MAPE is less than 3% for a standard deviation of 1%. This result demonstrates that the inverse-PINN method can learn the general Hamiltonian with good accuracy considering at least $N = 20$ collocation points, even though measurement errors are present. Also, we notice that the error in the inverse-PINN method increases with the number of differential equations and/or the number of parameters to be learned. If the interactions of N qubits are only between pairs, the MAPE for the whole system is equivalent to the error for a two-qubit system and thereby is not dependent on the number of qubits.

Although fundamental interactions between elementary particles are only between pairs, described by 2-local Hamiltonians, effective descriptions in multiple fields of interest, including condensed-matter physics, consider k -local Hamiltonians for convenience. A possible strategy to extract all coupling constants in Eq. (1), including up to N -body couplings, is to use the PINN and the FM by partitioning the learning procedure of the Hamiltonian. For example, with three qubits, a 3-local Hamiltonian involves up to $4^3 = 64$ terms. By successively using the FM to isolate one of the three qubits and the PINN on the remaining pair of qubits, we can extract 37 parameters. With the knowledge of these 37 parameters, we can now plug them into the differential equations and use the PINN to find the remaining 27 parameters,

this time turning off the freezing external fields. In general, for a system of N qubits containing all the terms of the N -local Hamiltonian, we have 4^N parameters. This number can be decomposed as follows:

$$4^N = \sum_{k=0}^N \frac{N!}{k!(N-k)!} 3^{N-k}. \quad (19)$$

Each term on the right-hand side corresponds to the number of parameters J_{k_1, k_2, \dots, k_N} that contain k zeros in their indexes. For instance, there are 3^N parameters if only interactions among all N qubits are considered ($k = 0$). For the general case, we can use the PINN together with the FM in a bottom-up approach. Thus, we first determine all 1-local and two-body parameters and then use these results to find the three-body coupling constants, and so on. In the final step, after determining all k -local terms for $k < N$, we apply the inverse PINN without the FM to determine the N -local term, utilizing the previously learned J constants.

Considering the case where only interactions between pairs are present, we can use the methodology for two qubits for the learning of an N -qubit system with the help of the FM. To explain how the freezing of qubits works, we use a four-qubit system coupled via next-nearest-neighbor interactions, described by the Hamiltonian

$$H = -\frac{1}{2} \sum_{k_1, k_2=0}^3 \sum_i (H_{k_1, k_2}^{(i, i+1)} + H_{k_1, k_2}^{(i, i+2)}), \quad (20)$$

where

$$H_{k_1, k_2}^{(j, l)} = L_{k_1, k_2}^{(j, l)} \sigma_{k_1}^{(j)} \sigma_{k_2}^{(l)}, \quad (21)$$

$L_{k_1, k_2}^{(j, l)}$ are the physical parameters to be learned, and the prime on the sum indicates that repeated terms are counted only once.

To freeze the interactions of the first and fourth qubits with both the second and third qubits, we have to add a strong and rapid oscillating external field that acts only in the first and fourth qubits described by the freezing Hamiltonian

$$H_F(t) = H_c^{(1)}(\omega_1, t) + H_c^{(4)}(\omega_4, t), \quad (22)$$

where

$$H_c^{(j)}(\omega_j, t) = \omega_j \sigma_3^{(j)} + 2\omega_j (\sin(2\omega_j t) \sigma_2^{(j)} + \cos(2\omega_j t) \sigma_1^{(j)}), \quad (23)$$

where $\omega_1 = \omega$ and $\omega_4 = 4\omega$. By using the freezing Hamiltonian of Eq. (22) together with the Hamiltonian of Eq. (20), we can isolate the second and third qubits from the other two qubits. In Fig. 3, we plot the difference between the expected values evaluated for the four- and two-qubit systems $\Delta_j = \langle \sigma_0^{(1)} \sigma_{k_j}^{(2)} \sigma_{k_j}^{(3)} \sigma_0^{(4)} \rangle - \langle \sigma_{k_j}^{(1)} \sigma_{k_j}^{(2)} \rangle$, $j = 1, 2$, and, 3, as a function of time for distinct values of ω . The values of $\langle \sigma_0^{(1)} \sigma_{k_j}^{(2)} \sigma_{k_j}^{(3)} \sigma_0^{(4)} \rangle$ are obtained by using the Hamiltonian of Eq. (20), while the values of $\langle \sigma_{k_j}^{(1)} \sigma_{k_j}^{(2)} \rangle$ come from having only the two-qubit system, which is obtained by Eq. (1) with $N = 2$. By employing the difference between the expected values evaluated for the four- and two-qubit systems with the same parameters related to the qubits of interest, we can infer the effects caused in the two-qubit system due to the coupling

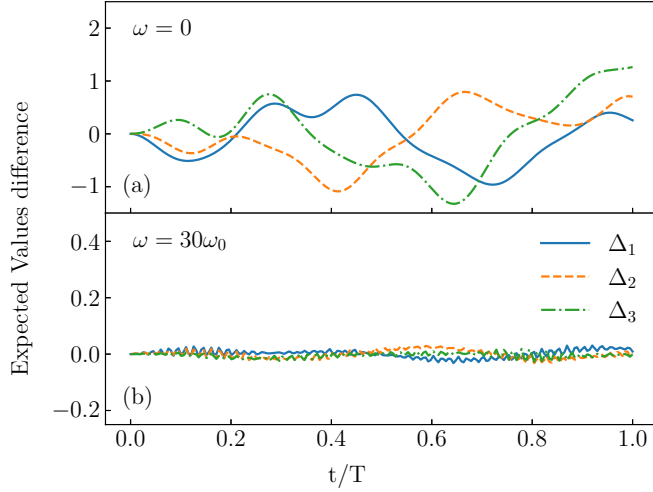


FIG. 3. The difference between the expected values evaluated for the four- and two-qubit systems $\Delta_j = \langle \sigma_0^{(1)} \sigma_{k_j}^{(2)} \sigma_{k_j}^{(3)} \sigma_0^{(4)} \rangle - \langle \sigma_{k_j}^{(1)} \sigma_{k_j}^{(2)} \rangle$, $j = 1, 2$, and 3 , as a function of time for distinct values of ω . Panel (a) considers $\omega = 0$, which shows that Δ_j achieves values bigger than 1, while panel (b) shows a drastic reduction of Δ_j due to the increasing of the value $\omega = 30\omega_0$, which is related to the freezing Hamiltonian.

with the first and fourth qubits. When the magnitude of the freezing Hamiltonian is $\omega = 0$ [Fig. 3(a)], one can notice that the first and fourth qubits strongly disturb the other two qubits due to their mutual coupling. On the other hand, the results for $\omega = 30\omega_0$ presented in Fig. 3(b) show that Δ_j is drastically reduced in comparison to the results obtained for $\omega = 0$. Thus, the first and fourth qubits decouple substantially from the other two qubits when the freezing Hamiltonian is present. Although we show the results only for three particular cases, similar behavior is found for all other qubit pairs. The values of Δ_j can be further reduced by increasing the value of ω . This result demonstrates that the learning of the Hamiltonian of Eq. (20) can be accomplished by freezing two qubits, determining the parameters of the other two qubits, and then repeating the process for all pairs of qubits. This computation can be parallelized once the experimental data have been collected.

In Fig. 4, we plot the MAPE distribution for the two qubits isolated from the four-qubit system as a function of the freezing Hamiltonian amplitude, ω/ω_0 . As expected, the values of the physical parameters of the Hamiltonian of the two qubits of interest are wrongly predicted if $\omega = 0$. As the amplitude of the freezing Hamiltonian increases, the prediction improves exponentially, demonstrating the feasibility of learning the parameters through the examination of the parts.

VI. APPLICATION TO IBM QUANTUM COMPUTER DATA

Finally, we simulate two different Hamiltonians H_Z and H_{XYZ} using the IBM quantum computer Lagos for generating the simulation data. The first Hamiltonian is given by

$$H_Z = -\frac{1}{2}(J_{0,3}\sigma_0^{(1)}\sigma_3^{(2)} + J_{3,0}\sigma_3^{(1)}\sigma_0^{(2)} + J_{3,3}\sigma_3^{(1)}\sigma_3^{(2)}), \quad (24)$$

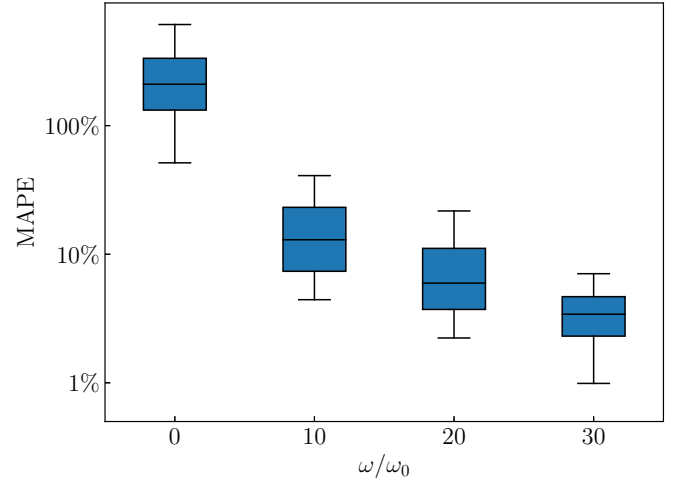


FIG. 4. The MAPE distribution of the prediction parameters $J_{k_1,k_2}^{(j,l)}$ for the four-qubit system as a function of ω/ω_0 considering $N = 20$ collocation points.

which has been used to fit experimental data related to quantum dots [20]. The second Hamiltonian is the XYZ model without local terms; thus,

$$H_{XYZ} = -\frac{1}{2}(J_{1,1}\sigma_1^{(1)}\sigma_1^{(2)} + J_{2,2}\sigma_2^{(1)}\sigma_2^{(2)} + J_{3,3}\sigma_3^{(1)}\sigma_3^{(2)}). \quad (25)$$

These two Hamiltonians have a simple quantum-gate representation and do not require any Trotter approximation. In Fig. 5, we plot the MAPE for H_Z and H_{XYZ} Hamiltonians as a function of the number of collocation points. The difference between these results and the previous ones [Fig. 2(a)] is related to the input data, which were obtained from the IBM quantum computer. For both Hamiltonians, using five collocation points, we find that the median of the MAPE achieves values less than 1% (see Fig. 5). By increasing the number of collocation points, the median values of the MAPE

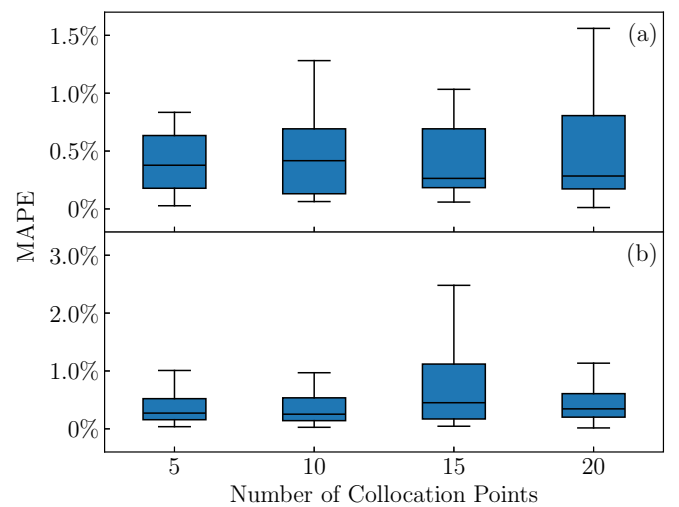


FIG. 5. The MAPE obtained from the data provided by the IBM quantum computer for (a) the H_Z Hamiltonian and (b) for the H_{XYZ} Hamiltonian as a function of the number of collocation points.

do not change substantially because the results have already converged for $N = 5$.

VII. CONCLUSIONS

Our procedure for learning a general Hamiltonian composed of N qubits is based on the inverse-PINN technique and the FM. In principle, all physical parameters could be directly determined by the inverse-PINN technique. Nonetheless, currently, the PINN is inefficient for a sufficiently large number of coupled differential equations and parameters. To circumvent this difficulty, we propose a mechanism to freeze the interactions from the surrounding qubits with a small part of the system. The small part of the system is used to extract the respective physical parameters and this procedure can be repeated until all parts have been probed. Here, we use a two-qubit system as a smaller unit, but bigger systems could be instead employed (e.g., see the case of three qubits in Appendix B). We found that the inverse-PINN method can determine the parameters of the two-qubit Hamiltonian with great accuracy when the input data are provided without errors, achieving a median error of less than 0.1%. By considering a Gaussian dispersion in the experimental data, we still can estimate the physical parameters with less than 2% accuracy on average, if we use at least 20 collocation points and a standard deviation in the input data of 1%. To demonstrate the feasibility of the whole procedure, we probed a four-qubit Hamiltonian, where the freezing external fields are applied to the first and fourth qubits, to reduce the interactions with the other two qubits. We verified that the FM successfully works when the amplitude of the freezing external fields is large enough to reduce the interactions with the qubits of interest.

Furthermore, use of the input data obtained from the IBM quantum computer for the H_Z and H_{XYZ} Hamiltonians provides a real test of this approach. In this practical case, we were able to determine very accurate physical parameters. For both Hamiltonians, using five collocation points, we achieved a median error of less than 1%. The integration of the FM with the inverse PINN presents a robust approach for acquiring the general Hamiltonian of an N -qubit system, with potential applications extending beyond its primary domain. For example, the inverse-PINN method holds promise for crosstalk detection [21], while the FM shows potential for crosstalk mitigation [22]. This approach can also be extended to learning a Hamiltonian composed of qudits through the use of the generalized continuous dynamical decoupling technique, primarily developed to protect the action of an arbitrary multiqubit gate from noise [18].

ACKNOWLEDGMENTS

The authors are grateful for financial support from the Brazilian Agencies FAPESP, CNPq, and CAPES. L.K.C., R.d.J.N., and F.F.F. thank the Brazilian Agency FAPESP (Grants No. 2019/09624-3, No. 2018/00796-3, No. 2021/04655-8, and No. 2023/04987-6) and also National Institute of Science and Technology for Quantum Information (CNPq INCT-IQ, Grant No. 465469/2014-0) for supporting this research. F.S.L. thanks the UNICAMP Postdoctoral

Researcher Program for financial support. F.F.F. also acknowledges support from ONR, Project No. N62909-24-1-2012.

APPENDIX A: DETAILS ABOUT THE FREEZING MECHANISM

To understand the FM, we consider, for a specific qubit, the freezing unitary operator factor, Eq. (6), acting on each Pauli matrix. This task becomes clearer in the interaction picture. Thus, in general, one finds that

$$[U_s^{(j)}(\omega_j, t)]^\dagger \sigma_{k_j}^{(j)} U_s^{(j)}(\omega_j, t) = \sum_{n_j=-3}^3 \exp(i2n_j\omega_j t) C_{k_j, n_j}, \quad (\text{A1})$$

where C_{k_j, n_j} is a linear combination of the Pauli matrices for $n_j = \pm 1, \pm 2$, and ± 3 , with $C_{k_j, 0} \equiv 0$.

By employing the result of Eq. (A1) in Eq. (7), we get

$$\begin{aligned} H_I^m(t) &= \prod_{j=1}^m \left[\sum_{n_j=-3}^3 \exp(i2n_j\omega_j t) C_{k_j, n_j} \right] \\ &= \sum_{n_1, \dots, n_m=-3}^3 \exp\left(i2t \sum_{j=1}^m n_j \omega_j\right) C_{k_1, n_1} C_{k_2, n_2} \cdots C_{k_m, n_m}. \end{aligned} \quad (\text{A2})$$

To guarantee that this last Hamiltonian averages to zero in a period of π/ω , we choose the following relation:

$$\omega_j = 4^{j-1} \omega, \quad (\text{A3})$$

for a given ω . Then, the argument of the exponential term in Eq. (A2) is proportional to

$$\sum_{j=1}^m n_j \omega_j = \omega \sum_{j=1}^m n_j 4^{j-1}. \quad (\text{A4})$$

Because $n_j = \pm 1, \pm 2$, and ± 3 , for $j = 1, 2, \dots, m$, we clearly see that the number

$$\sum_{j=1}^m n_j 4^{j-1} \neq 0 \quad (\text{A5})$$

for any given choice of (n_1, n_2, \dots, n_m) , since this m -tuple represents a nonzero base-four integer. This sum could only be zero if all $n_j = 0$, for all $j = 1, 2, \dots, m$, but this is impossible because we have that $C_{k_j, 0} = 0$, for $k_j = 1, 2$, and 3 and $j = 1, 2, \dots, m$.

Now, we want to evaluate the Dyson's series for the evolution operator associated with $H_I^m(t)$, given by Eq. (12). The Hamiltonian $H_I^m(t)$ in Eq. (7) is a periodic function of period $\tau = \pi/\omega$; therefore,

$$\int_0^\tau dt H_I^m(t) = 0. \quad (\text{A6})$$

Since $H_I^m(t)$ is periodic, the relation

$$U_I^m(N\tau, 0) = [U_I^m(\tau, 0)]^N \quad (\text{A7})$$

is valid for any integer N .

By assuming that g is the largest magnitude among all parameters J_{k_1, k_2, \dots, k_m} , and by noticing that it takes a time on

the order of $1/g$ for the effects of the undesired interactions to become apparent, we fix the final time t as a few units of π/g , say

$$t = \nu\pi/g, \quad (\text{A8})$$

where $\nu \in \mathbb{N}$. By choosing $\omega = fg$, we get $t = \nu f\tau$. Moreover, we can relate the final time as a large enough number N of periods τ plus a fraction ε of the period; thus,

$$t = (N + \varepsilon)\tau \quad (\text{A9})$$

and

$$\nu f = N + \varepsilon, \quad (\text{A10})$$

where $0 \leq \varepsilon < 1$. By assuming the above relations, we find that

$$\begin{aligned} U_I^m(t, 0) &= U_I^m(\varepsilon\tau + N\tau, N\tau)[U_I^m(\tau, 0)]^N \\ &\approx \left[\mathbb{1} + O\left(\varepsilon \frac{\nu\pi}{N}\right) \right] \left[\mathbb{1} + O\left(\frac{\nu^2\pi^2}{N}\right) \right] \\ &\approx \mathbb{1} + O\left(\frac{1}{N}\right). \end{aligned} \quad (\text{A11})$$

This last result contains the important information about the FM; i.e., it affirms that the evolution operator $U_I^m(t, 0)$ is approximately the identity, if we choose a large enough number of periods τ , and that the frequency must be chosen to exceed the largest magnitude among all interactions we intend to freeze.

APPENDIX B: THREE-QUBIT HAMILTONIAN LEARNING BY THE INVERSE-PINN METHOD

Here, the results of the direct application of the inverse-PINN technique to a system composed of three qubits are shown. The Hamiltonian that we intend to learn is

$$H_Z = -\frac{1}{2} \sum_{k_1, k_2, k_3=0 \text{ or } 3} (J_{k_1, k_2, k_3} \sigma_{k_1}^{(1)} \sigma_{k_2}^{(2)} \sigma_{k_3}^{(3)}), \quad (\text{B1})$$

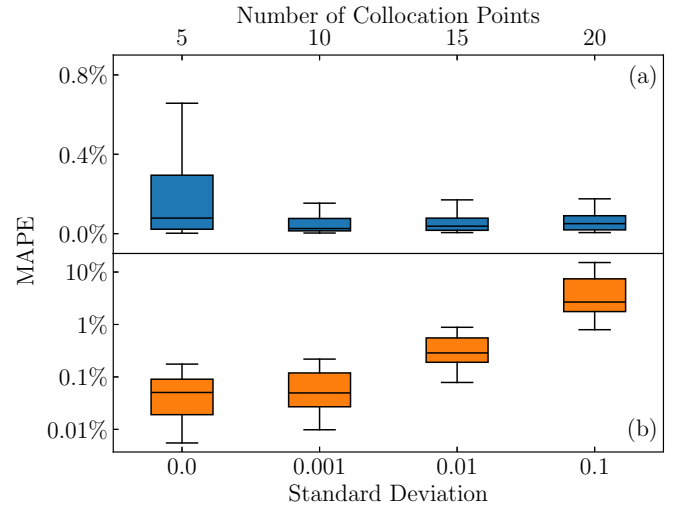


FIG. 6. The MAPE as function of the number of collocation points (a). The MAPE as a function of the standard deviation for $N = 20$ collocation points (b). Both related to the three-qubit Hz Hamiltonian [Eq. (B1)] with panel (b) plotted with a logarithmic scale.

where the last term of the summation accounts for three-body interactions.

In Fig. 6(a), we plot the MAPE as a function of the number of collocation points in time for the Hamiltonian of Eq. (B1). Figure 6(a) demonstrates that the median of the MAPE is lower than 0.04% for $N_c = 5$ collocation points. In Fig. 6(b), we use $N_c = 20$ collocation points and we include the random Gaussian error in the input data. In this case, we can see that the median of the MAPE is less than 3% for a standard deviation of 1%. This result demonstrates that the inverse-PINN method can learn the Hamiltonian for three qubits with good accuracy considering at least $N = 20$ collocation points, even though errors in the measurements are present. Of course, a higher accuracy can be attained by increasing the number of collocation points.

-
- [1] I. L. Chuang and M. A. Nielsen, *J. Mod. Opt.* **44**, 2455 (1997).
- [2] J. B. Altepeter, D. Branning, E. Jeffrey, T. C. Wei, P. G. Kwiat, R. T. Thew, J. L. O'Brien, M. A. Nielsen, and A. G. White, *Phys. Rev. Lett.* **90**, 193601 (2003).
- [3] S. T. Merkel, J. M. Gambetta, J. A. Smolin, S. Poletto, A. D. Córcoles, B. R. Johnson, C. A. Ryan, and M. Steffen, *Phys. Rev. A* **87**, 062119 (2013).
- [4] A. Anshu, S. Arunachalam, T. Kuwahara, and M. Soleimanifar, *Nat. Phys.* **17**, 931 (2021).
- [5] E. Bairey, I. Arad, and N. H. Lindner, *Phys. Rev. Lett.* **122**, 020504 (2019).
- [6] Z. Li, L. Zou, and T. H. Hsieh, *Phys. Rev. Lett.* **124**, 160502 (2020).
- [7] A. Zubida, E. Yitzhaki, N. H. Lindner, and E. Bairey, *arXiv:2108.08824*.
- [8] D. Hangleiter, I. Roth, J. Eisert, and P. Roushan, *arXiv:2108.08319*.
- [9] W. Yu, J. Sun, Z. Han, and X. Yuan, *Quantum* **7**, 1045 (2023).
- [10] S. T. Flammia and J. J. Wallman, *ACM Trans. Quantum Comput.* **1**, 1 (2020).
- [11] A. Gu, L. Cincio, and P. J. Coles, *Nat. Commun.* **15**, 312 (2024).
- [12] M. Raissi, P. Perdikaris, and G. Karniadakis, *J. Comput. Phys.* **378**, 686 (2019).
- [13] S. Wang, H. Wang, and P. Perdikaris, *Sci. Adv.* **7**, eabi8605 (2021).
- [14] L. Lu, X. Meng, Z. Mao, and G. E. Karniadakis, *SIAM Rev.* **63**, 208 (2021).
- [15] X. Xu, Z. Wang, C. Duan, P. Huang, P. Wang, Y. Wang, N. Xu, X. Kong, F. Shi, X. Rong *et al.*, *Phys. Rev. Lett.* **109**, 070502 (2012).

- [16] P. London, J. Scheuer, J.-M. Cai, I. Schwarz, A. Retzker, M. B. Plenio, M. Katagiri, T. Teraji, S. Koizumi, J. Isoya *et al.*, [Phys. Rev. Lett.](#) **111**, 067601 (2013).
- [17] Q. Guo, S.-B. Zheng, J. Wang, C. Song, P. Zhang, K. Li, W. Liu, H. Deng, K. Huang, D. Zheng *et al.*, [Phys. Rev. Lett.](#) **121**, 130501 (2018).
- [18] R. d. J. Napolitano, F. F. Fanchini, A. H. da Silva, and B. Bellomo, [Phys. Rev. Res.](#) **3**, 013235 (2021).
- [19] F. F. Fanchini, J. E. M. Hornos, and R. d. J. Napolitano, [Phys. Rev. A](#) **75**, 022329 (2007).
- [20] M. D. Shulman, O. E. Dial, S. P. Harvey, H. Bluhm, V. Umansky, and A. Yacoby, [Science](#) **336**, 202 (2012).
- [21] M. Sarovar, T. Proctor, K. Rudinger, K. Young, E. Nielsen, and R. Blume-Kohout, [Quantum](#) **4**, 321 (2023).
- [22] Z. Zhou, R. Sitler, Y. Oda, K. Schultz, and G. Quiroz, [Phys. Rev. Lett.](#) **131**, 210802 (2023).